Electronic Bistability in Linear Beryllium Chains

Wissam Helal,[†] Antonio Monari,*[,‡] Stefano Evangelisti,[†,§] and Thierry Leininger[†]

Laboratoire de Chimie et Physique Quantiques, UMR 5626, Université de Toulouse et CNRS, 118 Route de Narbonne, F-31062 Toulouse Cedex, France, and Dipartimento di Chimica Fisica e Inorganica, Università di Bologna, Viale Risorgimento 4, I-40136 Bologna, Italy

Received: January 22, 2009; Revised Manuscript Received: March 11, 2009

A theoretical investigation on the mixed-valence behavior (bistability) of a series of cationic linear chains composed of beryllium atoms, Be_N^+ (with $N = 6,..., 12$), is presented. The calculations were performed at CAS-SCF and MR-CI levels by using an ANO basis set containing 6s4p3d2f orbitals for each atom. Our results show a consistent gradual shift between different classes of mixed-valence compounds as the number of beryllium atoms increases, from class III strong coupling toward class II valence trapped. Indeed, in the largest cases ($N > 10$), the cationic chains were found to be closer to class I, where the coupling vanishes. The intramolecular electron transfer parameters V_{ab}, E_a, and E_{opt} were calculated for each atomic chain. It is shown that the decrease of V_{ab} with increasing N follows an exponential pattern.

1. Introduction

Mixed-valence compounds are characterized by intervalence charge transfer (CT) between two or more redox sites existing in different oxidation states. The great interest in mixed-valence compounds lays primarly in their use as model systems for the study of the ubiquitous electron-transfer (ET) phenomena.[1−3] In addition, these molecules are extensively investigated for their molecular electronic applications.[4−8] Robin and Day classified mixed-valence compounds into three categories,[9] (a) the redox centers are completely localized where there is no electronic coupling between the redox centers (class I), (b) intermediate electronic coupling between the mixed-valence centers exists, and the charge is partly localized in one redox center (class II), and finally, (c) class III derivatives where coupling is so strong that the system is completely delocalized and intermediate redox states have to be attributed to the redox centers. The transition between class II and class III systems has recently attracted considerable attention.[10−13]

According to Marcus,[14−16] the potential energy surface (PES) of a degenerate mixed-valence system can be constructed from parabolic functions, each representing a diabatic, noninteracting, state; see Figure 1. In the case of two interacting states a and b, the electronic interaction (coupling) between these states will mix their wave functions with each other, to an extent that depends on the magnitude of the interaction. This leads to an effective removing of the degeneracy at the crossing of the diabatic wave functions, that is, the formation of the avoided crossing, which gives rise to two new and separate adiabatic states of energies E^1 and E^2 (defined below). A typical symmetric PES showing two adiabatic states that resulted from a coupling of two diabatic states is sketched in Figure 1. The electronic coupling V_{ab}, known as the coupling matrix element, is defined as half of the splitting between the adiabatic potential energy surfaces E^1 and E^2 at the crossing seam (see Figure 1)

$$2V_{ab} = E^2 - E^1 \quad (1)$$

where E^1 and E^2 in the most simple model (a two-state model) can be represented as the solutions of a 2×2 secular equation.[15,17] For class II systems, two intramolecular electron-transfer pathways are conceivable.[18]

(1)A thermal process where the system moves from one minimum of the lower adiabatic surface over a transition state along the electron-transfer coordinate to the other minimum. The activation energy of this transition is the adiabatic energy barrier separating the two equilibrium points, E_a.

(2)An optical process where the system is photoexcited from one minimum of the lower adiabatic surface to the Franck−Condon state of the upper adiabatic surface. The energy of this excitation is the Marcus reorganization energy λ and is equal to the optical transition energy, E_{opt}, in the case of symmetric PES's.

It is worthwhile to mention that for more complex systems, this simple model may not correctly represent the mixed-valence and ET parameters, and other more complicated models are required for a proper modeling of these systems.[19,20]

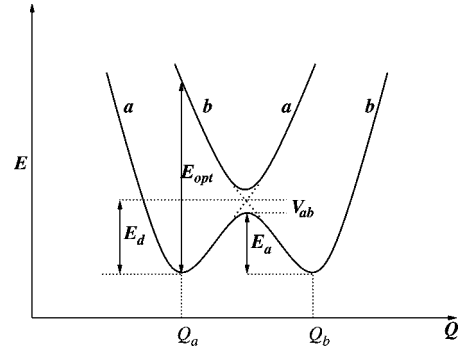

Figure 1. A cross section of an energy profile for initial state a and final state b in a typical symmetric (exothermicity or $\Delta E = 0$) ET reaction. The solid curves are the adiabatic surfaces, and the dashed lines refer to diabatic surfaces. Q_a and Q_b are equilibrium nuclear coordinates *of* *a* and b, respectively. The electron transfer matrix V_{ab}, diabatic activation energy E_d, adiabatic activation energy E_a, and E_{opt} are indicated.

* To whom correspondence should be addressed. Email: amonari@ms.fci.unibo.it.
[†] Université de Toulouse et CNRS.
[‡] Università di Bologna.
[§] E-mail: stefano@irsamc.ups-tlse.fr.

10.1021/jp900663p CCC: $40.75
Published on Web 03/31/2009

In this Article, we investigate the possible presence of mixed-valence behavior inducing bistability. For the sake of simplicity, isolated chains only will be considered here, although we plan in the future to investigate surface-deposed chains and more complex systems. The construction of individual atomic metal chains precisely deposed on nanosurfaces was experimentaly made possible by the advent of new nanotechnological techniques such as the scanning tunneling microscopy (STM)[21−25] and other combined techniques.[26,27] While gold atomic chains have received considerable attention,[26−28] other metallic chains have also been investigated.[29,30] These atomic metal chains present interesting one-dimensional electronic properties.[28,31−33] As an example, atomic metallic chains are characterized by edge orbitals that can be considered as the analogues of surface states.[34]

In previous studies, we investigated the electronic structure of neutral berylliun chains.[35−37] It was found that close to the equilibrium geometry, these systems present two singly occupied equivalent edge orbitals, located at the chain extremities. Because of their very weak interaction, these orbitals give rise to two quasi-degenerate states, a singlet and a triplet. If an electron is extracted from the system and the chain length is sufficiently long, the resulting hole will localize in one of the two edge orbitals. This induces an asymmetric distortion of the geometric framework of the chain and the formation of a mixed-valence system.

In the present contribution, the structure of a series of cationic beryllium chains, Be_N^+ (with $N = 6,..., 12$), has been computed at complete active space self-consistent field (CAS-SCF) and multi-reference configuration interaction (MR-CI) levels. In particular, it was found that the extent of the charge localization, and thus the bistability, of a beryllium chain cation depends exclusively on the number of the atoms constituting the chain. The nature of this dependency is addressed in this work. CAS-SCF and MR-CI calculations were applied to the beryllium cationic chains in order to compute the intramolecular charge-transfer parameters, namely, $2V_{ab}$, E_a, and E_{opt}, of the systems under investigation. It should be mentioned that, to the best of our knowledge, this is the first study that explicitly considers the mixed-valence nature of atomic chain cations.

2. Linear Beryllium Chains

Beryllium and other atomic linear chains have been recently investigated by our group.[35−39] Here, we briefly recall the structure of neutral beryllium chains. At large distances, the beryllium atoms are essentially isolated atoms in their ground state, and the system is weakly bound by dispersion (van der Waals) interactions. This fact is confirmed by the structure of the valence orbitals, which are essentially symmetry combinations of the 2s orbitals of the beryllium atoms. At a distance of about 5.5 bohr, the wave function experiences a rapid change toward a totally different structure. Two singly occupied edge orbitals are present at the chain extremities. This is the result of the formation, in the direction of the chain axes (say, z), of two sp_z hybrid orbitals on each Be atom. By combining these hybrid orbitals, Be−Be single σ bonds are formed between adjacent atoms. Globally, there are $N - 1$ of these σ bonds, and they host $2N - 2$ out of the $2N$ valence electrons of the system. The two remaining valence electrons are placed into the two terminal (edge) hybrid orbitals that do not combine themselves with any other valence orbital. Being equivalent and located in different regions of the molecule, they are quasi-degenerate. Hence, they give rise to two quasi-degenerated low-lying states, a singlet and a triplet.

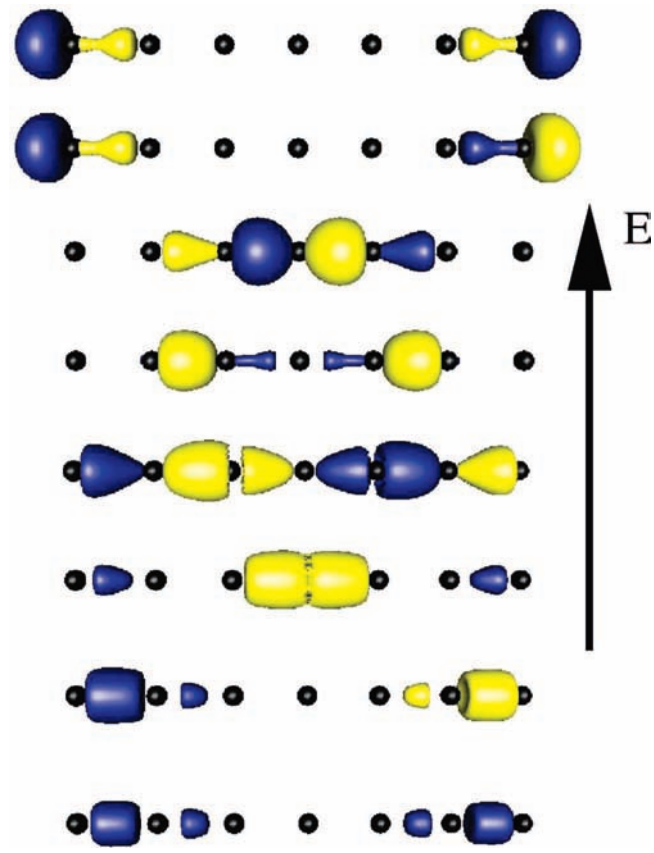

Figure 2. The occupied valence and active orbitals of Be_7^+ at the D_{2h} (symmetric) geometry, produced at the CAS-SCF(1/2) level using the ANO basis set (6s,4p,3d,2f).

The extraction of an electron from a neutral chain will leave the cation charge localized in one of the two edges of the linear chain, thus potentially inducing a deformation of the chain geometry. As previously stated, this will be reflected by the possible formation of a bistable (a double-well) electronic ground-state PES or, in other words, the formation of a mixed-valence system of class II. The symmetry of a neutral linear Be_N chain is $D_{\infty h}$, where the principal axis of rotation, C_∞, passes through all of the beryllium atoms. The ground electronic state geometry of the distorted cations shows two equivalent minima having $C_{\infty v}$ symmetry. The two minima are separated by a saddle point at the crossing seam with a symmetric $D_{\infty h}$ geometry. In the following, the orbitals designation and the symmetry states of $D_{\infty h}$ and $C_{\infty v}$ point groups will be discussed in terms of D_{2h} and C_{2v} symmetry elements and point groups respectively (see section 3, Computational Details). The occupied valence orbitals of Be_7^+ at D_{2h} and C_{2v} geometries are shown in Figures 2 and 3, respectively. Contrary to the D_{2h} case, the highest two occupied molecular orbitals (MOs) of the C_{2v} systems are completely localized, each one at one of the borders of the Be_7^+ chain. The highest occupied molecular orbital (HOMO) and the lowest unoccupied molecular orbital (LUMO) are chosen as the active space orbitals for all of the beryllium chain cations in the CAS-SCF and MR-CI calculations.

3. Computational Details

ROHF, CAS-SCF, and contracted MR-CI (C-MR-CI)[40,41] were obtained for the system of Be_N^+ ($N = 6−12$) using MOLPRO code version 2002.6.[42] Since the MOLPRO code can only treat Abelian point groups, all calculations were performed using the C_{2v} or D_{2h} symmetry point group instead of $C_{\infty v}$ and

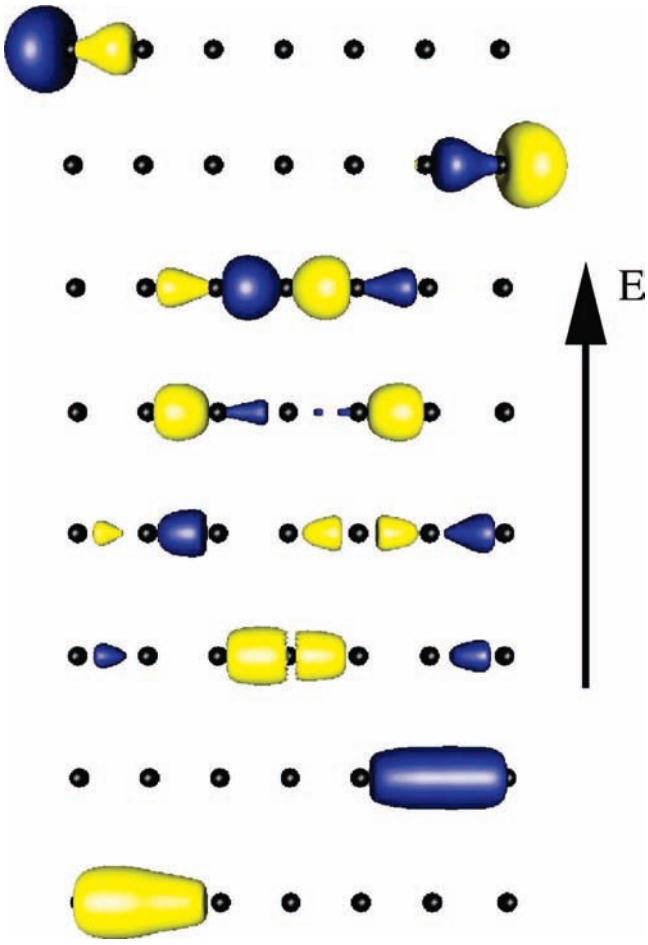

Figure 3. The occupied valence and active orbitals of Be_7^+ at the C_{2v} (unsymmetric) geometry, produced at the CAS-SCF(1/2) level using the ANO basis set (6s,4p,3d,2f). The electron hole is localized in the terminal bond at the left side of the chain.

$D_{\infty h}$, respectively. However, for convenience, the geometry of the saddle point (of D_{2h} symmetry) was performed by MOLPRO using the C_{2v} subgroup. The orbital density isosurface plots were obtained by using gOpenMol version 2.3.[43] Geometry optimization, single point calculations, and potential energy surfaces for the whole series of Be_N^+ were computed using the atomic natural orbitals (ANO)[44] basis set with 6s, 4p, 3d, and 2f for each beryllium atom. The active space was chosen in such a way to include the HOMO (see Figure 3) and the LUMO for each chain, both for D_{2h} and C_{2v} geometries. For all of the cationic chains, the two active orbitals would be occupied by a single active electron, hence the designation CAS(1/2). The same active orbitals were used for C-MR-CI calculations.

In order to avoid PES discontinuity at the saddle point, state-averaged CAS-SCFs were computed for the $^2A_1$ states of Be_N^+ chains. Two state-averaged $^2A_1$ state were computed, namely, 1^2A_1 and 2^2A_1. As a first step, geometry optimizations of Be_N^+ chains at the equilibrium, C_{2v} geometries, and at transition states, D_{2h} geometries, were performed at the ROHF level. These geometries were used to construct the reaction coordinates of all of the series of Be_N^+ chains.

The reaction paths were obtained by averaging the geometries of two points on the reaction coordinates according to a mixing parameter ξ.[45] The simplest choice is to mix linearly the geometries of the two (equivalent) optimized minima. This choice will produce smooth curves on the whole ξ range, including the crossing seam, and it will make it possible to test the geometries of the transition states on the reaction coordinates with respect to the truly optimized transition-state geometries. The geometries along the reaction coordinate have been calculated using the formula[45]

$$Q(\xi) = \left(\frac{1}{2} - \xi\right)Q_A + \left(\frac{1}{2} + \xi\right)Q_B \qquad (2)$$

where $Q(\xi)$ is the nuclear configuration at the point ξ on the reaction path, while Q_A and Q_B represent the nuclear coordinates of the two optimized (equivalent) C_{2v} geometries. The mixing parameter ξ was varied from -1.00 to $+1.00$ in steps of 0.05. For large values of N, the crossing is weakly avoided. Therefore, for $N = 10-12$, smaller steps of 0.01 were used in the range of -0.05 to $+0.05$ in order to obtained smooth curves. In this model, Q_A (the geometry of the first C_{2v} minimum) corresponds to the point $\xi = -0.50$, Q_B (the geometry of second C_{2v} minimum) corresponds to the point $\xi = +0.50$, and the averaged D_{2h} geometry corresponds to the crossing seam at $\xi = 0.00$. The Born−Oppenheimer potential energy surfaces were obtained by calculating the energies of 1^2A_1 and 2^2A_2 electronic states for each step value of the parameter ξ using CAS-SCF and C-MR-CI methods.

In order to test the quality of the reaction coordinate, the energy of the optimized D_{2h} geometry was compared with the corresponding energy computed at $\xi = 0.00$. The results show a very small energy difference between the averaged and the optimized D_{2h} geometries. As an example, for the beryllium chain where $N = 7$, the optimized D_{2h} geometry was 0.504 kJ/mol lower than that of the averaged D_{2h} Be_7^+ geometry at $\xi = 0.00$. In addition, a comparison of the corresponding bond lengths of the chains at the averaged and optimized D_{2h} geometries also shows an extremely small difference between the two structures. Considering the same chain (i.e., Be_7^+), the bond length values of bond 1 are 4.228 and 4.186 bohr for averaged and optimized D_{2h} geometries, respectively. The difference between bond lengths of the other bonds of averaged and optimized D_{2h} Be $_7^+$ geometries were even smaller than that of bond 1, and the same is true for the other atomic beryllium chains. For these reasons, we believe that the geometry path obtained through eq 2 is very close to the optimal one. This is not surprising if one considers the relatively small distortion of the chain geometry when the hole moves from one extremity to the opposite one. More complex systems are likely to present a very different behavior.

The $2V_{ab}$ values were computed by using eq 1 as the difference between the energies of 1^2A_1 and 2^2A_2 adiabatic states at the crossing seam, $\xi = 0.00$. The E_a values were computed by subtracting the adiabatic state energies of the 1^2A_1 state at the crossing seam, $\xi = 0.00$, and the equilibrium geometry, $\xi = 0.50$. Finally, the E_{opt} values were computed by subtracting the adiabatic state energies of the 1^2A_1 and 2^2A_2 states at the equilibrium geometry, $\xi = 0.50$.

4. Results and Discussion

The bond lengths of the optimized Be_N^+ chain equilibrium geometries are presented in Table 1. Bond numbering scheme can be summarized as follows: bond number 1 is the terminal bond on the "cationic" side, that is, the side where the charge is localized; bond 2 is the bond adjacent to bond 1; and so forth. In this way, the last bond for each chain (bond $N - 1$) is the terminal bond on the "neutral" side. When looking at the bond lengths of Be_N^+ collected in Table 1, one can immediately notice the strong geometry deformation of all of the beryllium chains

TABLE 1: Bond Lengths, in bohr, of Optimized Be_N^+

	bond length of Be_N^+						
bond no.	$N = 6$	$N = 7$	$N = 8$	$N = 9$	$N = 10$	$N = 11$	$N = 12$
1	4.359	4.364	4.366	4.368	4.368	4.369	4.369
2	4.139	4.143	4.146	4.147	4.147	4.147	4.148
3	4.088	4.094	4.097	4.098	4.099	4.099	4.100
4	4.076	4.087	4.092	4.094	4.095	4.095	4.096
5	4.086	4.083	4.093	4.097	4.099	4.100	4.101
6		4.093	4.089	4.098	4.103	4.105	4.106
7			4.105	4.093	4.102	4.106	4.108
8				4.102	4.096	4.105	4.109
9					4.105	4.097	4.106
10						4.106	4.098
11							4.108

and, therefore, the strong localization of the cation charge in a terminal bond of a chain. For instance, the terminal "cationic" bond (bond 1) of Be_6^+ has a length of 4.359 bohr, while the bonds 3−5 are very close in value, ranging from 4.076 to 4.088 bohr. Results in Table 1 show clearly that, for a single chain, bond length changes for bond numbers >2 are very small, while a significant change is observed for bond 1. It is worthwhile to note that bonds numbered 2 are slightly more "cationic", that is, longer, than bonds numbered 3 to $N - 1$ but significantly less than bond 1. It is also interesting to note that the deformation of bond 1 is almost constant with N. As an example, we can see that for bond number 1, the length is 4.359 bohr for $N = 6$ and 4.369 bohr for $N = 12$. Similar behaviors can be found for the other bonds.

CAS-SCF and MR-CI potential energy surfaces as a function of ξ for Be_N^+, are shown in Figures 4 and 5, respectively. The figures show PES for $N = 6-10$. These plots represent the adiabatic surfaces of the Be_N^+ chains where, for each chain, the lower electronic ground state is the 1^2A_1 state, by using the corresponding C_{2v} symmetry elements, and the higher first excited electronic state is the 2^2A_2 state. The absolute atomic unit energies of all of the electronic states were scaled in such a way to set the zero of the energy scale to the middle point of the splitting between the ground and first excited states at the crossing seam, $\xi = 0$. The values of $2V_{ab}$, E_a, and E_{opt} for Be_N^+ chains using CAS-SCF and MR-CI are presented in Table 2.

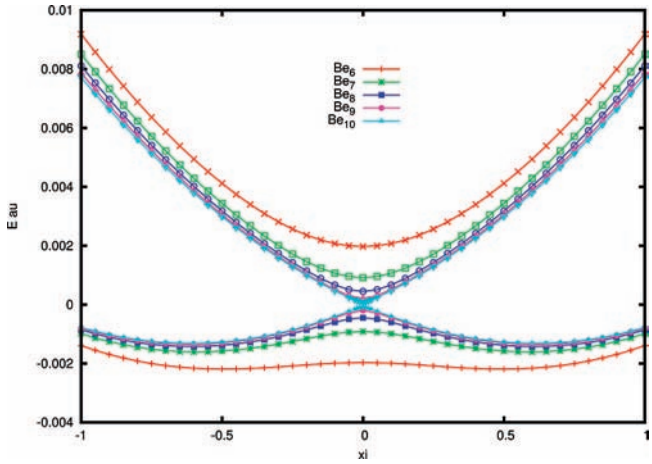

Figure 4. Adiabatic potential energy surfaces of Be_N^+ ($N = 6-10$) for the ground electronic states 1^2A_1 and the first excited states 2^2A_1. Energies in au (see the text), produced at CAS-SCF, as a function of ξ.

A consistent gradual shift toward valence trapping, or bistability, from $N = 6$ to 12 is observed. The Be_N^+ chains tend to move from class III to class I, passing by class II, mixed-valence systems, while increasing the number of beryllium atoms N in a chain. This is true for both CAS-SCF and MR-CI calculations, as shown in Figures 4 and 5, although the bistability is more pronounced at the CAS-SCF level. For instance, for $N = 6$, a very weak valence trapping, or charge localization, is observed since the values of $2V_{ab}$ are relatively large and those of E_a are very small (the energy barrier actually disappears in the case of $N = 6$ using a MR-CI calculation). On the other hand, beryllium chains with far higher N, say 10−12, have relatively high energy barrier E_a values and relatively low electronic coupling $2V_{ab}$ values; see Table 2.

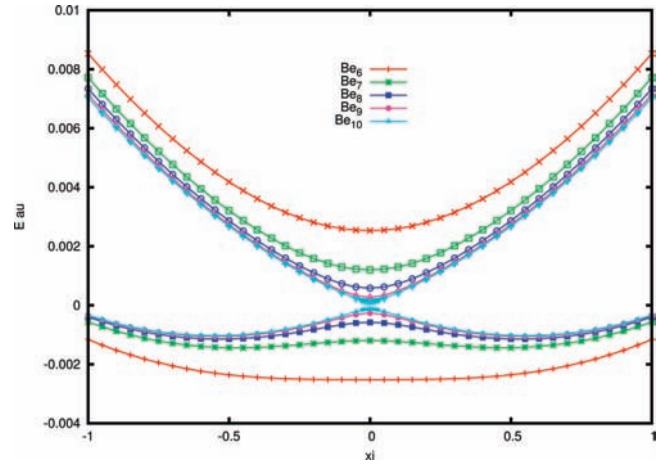

Figure 5. Adiabatic potential energy surfaces of Be_N^+ ($N = 6-10$) for the ground electronic states 1^2A_1 and the first excited states 2^2A_1. Energies in au (see the text), produced at C-MR-CI, as a function of ξ.

TABLE 2: $2V_{ab}$, E_a, and E_{opt} Energy Values, in kJ/mol, of Be_N^+

method	N	$2V_{ab}$	E_a	E_{opt}
CAS-SCF	6	10.356	−0.577	16.567
	7	4.813	−1.741	13.174
	8	2.340	−2.466	11.980
	9	1.066	−2.899	11.452
	10	0.548	−3.066	11.190
	11	0.226	−3.172	11.018
	12	0.137	−3.182	10.919
MR-CI	6	13.276	0.441	17.181
	7	6.299	−0.628	12.202
	8	3.040	−1.487	10.527
	9	1.398	−2.061	9.936
	10	0.694	−2.336	9.721
	11	0.296	−2.503	9.613

The MR-CI results, when compared with those of CAS-SCF, tend to slightly decrease the energy separation between the adiabatic ground state 1^2A_1 and the first excited electronic state 2^2A_2 ($2V_{ab}$) for each N, as shown in Table 2. As far as the activation energy E_a is concerned, on the contrary, the inclusion of dynamic correlation seems to decrease the barrier at the crossing seam.

The relationship between the coupling V_{ab} and the number of beryllium atoms N in a chain has been considered. The two quantities obey to an exponential relationship

$$V_{ab}(N) = V_{ab}^0 e^{-\alpha N} \quad (3)$$

where V_{ab}^0 is a constant. A plot of log $2V_{ab}$ as a function of N is shown in Figure 6. An overall linear behavior is observed,

confirming the previous relationship. However, slight deviations from linearity appear for the highest N values. By plotting log $2V_{ab}$ as a function of even and odd N values separately, one obtains a far better linear behavior even for high N values; this is demonstrated in Figure 7, where plots of log $2V_{ab}$ as a function of even and odd N plots at the CAS-SCF level are shown. The same behavior was also obtained at the MR-CI level. Table 3 reports the values of α obtained by a least-squares fitting of log V_{ab} as a function of N for CAS-SCF and MR-CI methods and for even and odd values of N. It is important to mention that the general exponential behavior of $2V_{ab}$ may be attributed to the absence of chemical substituents. This situation is in contrast with the case of most organic and inorganic mixed-valence systems, where the substituent could contribute directly to the thermal ET process (through bond ET). A complete investigation of this point is beyond the scope of this work.

Finally, the vertical electron affinity of the cation was considered. It is defined as $E(Be_N^+) - E(Be_N)$, computed at the optimized cation geometry, and it is, in this way, a positive quantity. In Table 4, the dependence of the electron affinity with N is reported. It appears that by augmenting the number of atoms in the chain, the electronic affinity becomes smaller. The weak dependence on N, however, confirms the very localized nature of the hole. The values are illustrated in Figure 8. The MR-CI values are larger (about 5%) than the corresponding CAS-SCF results. This is consistent with the presence of a larger dynamical correlation energy in the neutral species than that in the ions, a common fact in CI calculations. There is also a tiny increase of the EA by going from the symmetric $D_{2\infty}$ geometry to the distorted $C_{2\infty}$ one, probably due to the less diffuse character of the singly occupied edge orbital in the distorted geometry with respect to that in the symmetric one.

The present results suggest the possibility of using cationic linear chains of beryllium atoms as electronic "charge-transfer" devices, in which intramolecular charge-transfer parameters, for example, V_{ab}, could be directly controlled, or "designed", by varying the number of atoms of the chain.

This aspects could imply the necessity of performing high-level computations on linear chains of different atoms absorbed on nanostructures. To achieve this target, the use of local MRCI methods[46,47] is highly desirable. Moreover, the study of organic or inorganic mixed valence systsems[48] would be of great interest. Even if, in this case, the increased size of the system under examination would certainly lead to a more difficult interpretation of the results and to a highly increased computational cost.

5. Conclusions

It has been shown that linear beryllium chains behave like mixed-valence systems when one electron is removed from the system. An increase of mixed-valence character (bistability or charge localization) with increasing the number of beryllium atoms N in a cationic chain has been evidenced. As expected in the case of extended mixed-valence systems, there is a decreasing V_{ab} with increasing N. In particular, a linear relationship between log $2V_{ab}$ and the number of beryllium atoms (N) has been found. Indeed, at the equilibrium geometry, the chain length is, to a very good extent, directly proportional to the number of atoms. This fact justifies the exponential relationship between $2V_{ab}$ and the chain length, consistent with the fact that in the cation, the hole is located in one of the two edge orbitals.

These results are particularly interesting for at least two reasons. First of all, mixed-valence systems could be used to design interesting devices, particularly in the field of molecular electronics. A promising possibility would be to deposit beryllium chains on nanodevices (on top of graphene surfaces and nanorods or inside of nanotubes) in order to exploit the mixed-valence nature of the cation. The possibility of going from class I to class III in a tunable way, by simply changing the number of atoms in the chain, makes these systems

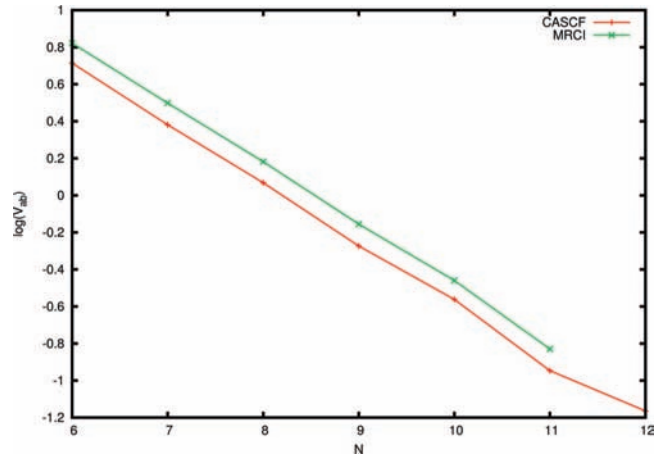

Figure 6. Log $2V_{ab}$, calculated at CAS-SCF and C-MR-CI, as a function of the number of beryllium atoms N.

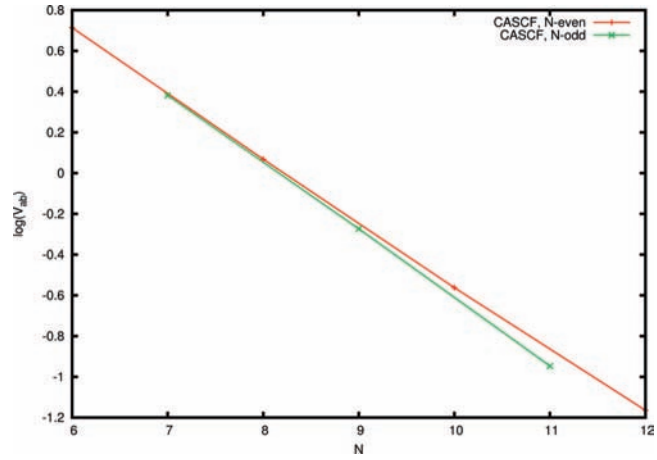

Figure 7. Log $2V_{ab}$, calculated at CAS-SCF as a function of even and odd N.

TABLE 3: Least-Square Fitted Values of α (see text for details) along with the Correlation Coefficient ρ

	CAS-SCF	MR-CI	CAS-SCF even N	CAS-SCF odd N	MR-CI even N	MR-CI odd N
α	−0.734	−0.755	−0.721	−0.765	−0.738	−0.764
ρ	0.9989	0.9997	0.9998	0.9999	0.9999	0.9999

TABLE 4: Electronic Affinities, in kJ/mol, of Be_N^+ Optimized at the Cation Geometries for D_{2h} and C_{2v} Geometries Both at CASSCF and MRCI

	Electronic Affinities			
	CASSCF		MRCI	
N	D_{2h}	C_{2v}	D_{2h}	C_{2v}
6	556.397	551.612	588.426	585.297
7	555.306	549.337	585.807	581.540
8	553.952	547.318	583.151	578.022
9	552.808	545.801	580.839	575.143
10	551.827	544.696	578.824	572.855
11	551.109	543.909	577.178	571.043
12	550.516	543.324		

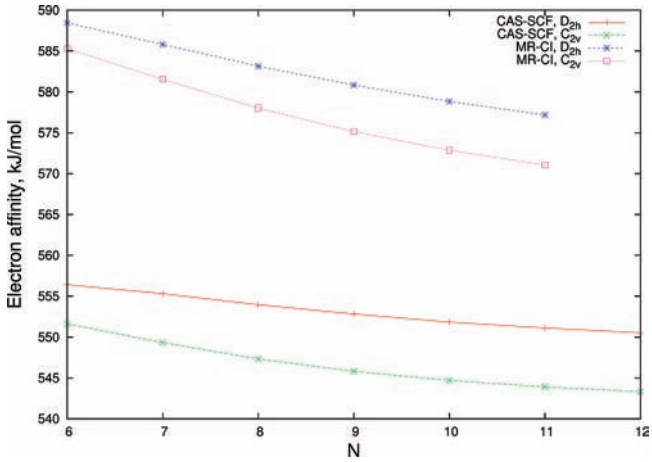

Figure 8. Electronic affinities, in kJ/mol, of the cationic Be_N^+ as a function of the number of atoms N in a chain.

particularly attractive. Moreover, as isolated objects, beryllium chains are relatively simple systems. For this reason, they are particularly adapted to assess the quality of the theoretical methods used to perform these studies.

Finally, it is worth mentioning that preliminary investigations on neutral atomic chains containing atoms of the Groups 2 and 12 seem to indicate that the presence of edge orbitals is not restricted to beryllium alone. If these results were confirmed by subsequent investigations, the number of possibilities for mixed-valence atomic chains would be extremely large. Although the stability of isolated chains toward collapse into more stable compact clusters is still to be investigated, linear structures could perhaps be stabilized by deposition on inert surfaces. This possibility, combined with the remarkable predicted properties of the neutral chains, could open interesting perspectives in the fast-growing field of nanodevices.

Acknowledgment. This work was supported by the French "Centre National de la Recherche Scientifique" (CNRS), the Italian Ministry of University and Research (MUR), and the University of Bologna under the Project "PRIN 2006. Molecular Quantum Mechanics: Computational Methods and Analysis of Novel Phenomena". Support from the European Community under the COST D37 action (GRIDCHEM) is also gratefully acknowledged.

References and Notes

(1) Creutz, C. *Prog. Inorg. Chem.* **1983**, *30*, 1.
(2) Richardson, D. E.; Taube, H. *Coord. Chem. Rev.* **1984**, *60*, 107.
(3) Barbara, P. F.; Meyer, T. J.; Ratner, M. A. *J. Phys. Chem.* **1996**, *100*, 13148.
(4) Joachim, C.; Gimzewski, J. K.; Aviram, A. *Nature (London)* **2000**, *408*, 541.
(5) Fraysse, S.; Coudret, C.; Launay, J.-P. *Eur. J. Inorg. Chem.* **2000**, *1*, 1581.
(6) Barigelletti, F.; Flamigni, L. *Chem. Soc. Rev.* **2000**, *29*, 1.
(7) Lukas, A. S.; Bushard, P. J.; Wasielewski, M. R. *J. Am. Chem. Soc.* **2001**, *123*, 2440.
(8) Braun-Sand, S. B.; Wiest, O. *J. Phys. Chem. B* **2003**, *107*, 9624.
(9) Robin, M.; Day, P. *Adv. Inorg. Radiochem.* **1967**, *10*, 247.
(10) Nelsen, S. F. *Chem.—Eur. J.* **2000**, *6*, 581.
(11) Demadis, K. D.; Hartshorn, C. M.; Meyer, T. J. *Chem. Rev.* **2001**, *101*, 2655.
(12) Brunschwig, B. S.; Creutz, C.; Sutin, N. *Chem. Soc. Rev.* **2002**, *31*, 168.
(13) D'Alessandro, D. M.; Keene, R. *Chem. Soc. Rev.* **2006**, *35*, 424.
(14) Marcus, R. A.; Sutin, N. *Biochim. Biophys. Acta* **1985**, *811*, 265.
(15) Sutin, N. *Prog. Inorg. Chem.* **1983**, *30*, 441.
(16) Creutz, C.; Newton, M. D.; Sutin, N. *J. Photochem. Photobiol., A* **1994**, *82*, 47.
(17) Newton, M. D.; Sutin, N. *Annu. Rev. Phys. Chem.* **1984**, *35*, 437.
(18) Hush, N. S. *Coord. Chem. Rev.* **1985**, *64*, 135.
(19) Fernández, E.; Blancafort, L.; Olivucci, M.; Robb, M. *J. Am. Chem. Soc.* **2000**, *122*, 7528.
(20) Blancafort, L.; Fernández, E.; Olivucci, M.; Robb, M. *J. Am. Chem. Soc.* **2001**, *123*, 722.
(21) Stipe, B. C.; Resaei, M. A.; Ho, W. *Science* **1998**, *280*, 1732.
(22) Weiss, P. S.; Yokota, H.; Allara, D. L. *J. Phys.: Condens. Matter* **1998**, *10*, 7703.
(23) Gimzewski, J. *Phys. World* **1998**, *11*, 29.
(24) Andres, R. P.; Bielefeld, J. D.; Henderson, J. I.; Janes, D. B.; Kolagunta, V. R.; Kubiak, C. P.; Mahoney, W. J.; Osifchin, R. G. *Science* **1996**, *273*, 1690.
(25) Bumm, L. A.; Arnold, J. J.; Cygan, M. T.; Dunbar, T. D.; Burgin, T. P.; Jones, L., II; Allara, D. L.; Tour, J. M.; Weiss, P. S. *Science* **1996**, *271*, 1705.
(26) Ohnishi, H.; Kondo, Y.; Takayanagi, K. *Nature (London)* **1998**, *395*, 780.
(27) Rubio-Bollinger, G.; Bahn, S. R.; Agraït, N.; Jacobsen, K. W.; Vieira, S. *Phys. Rev. Lett.* **2001**, *87*, 026101.
(28) Crain, J. N.; Pierce, D. T. *Science* **2005**, *307*, 703.
(29) Bahn, S. R.; Jacobsen, K. W. *Phys. Rev. Lett.* **2001**, *87*, 266101.
(30) Amorim, E. P; da Silva, A. J. R.; Fazzio, A.; da Silva, E. Z. *Nanotechnology* **2007**, *18*, 145701.
(31) Emberly, E. G.; Kirczenow, G. *Phys. Rev. B* **1999**, *60*, 6028.
(32) Himpsel, F. J.; Altmann, K. N.; Bennewitz, R.; Crain, J. N.; Kirakosian, A.; Lin, J.-L.; McChesney, J. L. *J.Phys.: Condens. Matter* **2001**, *13*, 11097.
(33) Nilius, N.; Wallis, T. M.; Ho, W. *Science* **2002**, *297*, 1853.
(34) Davidson, S. G.; Stślicka, M. *Basic Theory of Surface States*; Clarendon: Oxford, U.K., 1992.
(35) Monari, A.; Vetere, V.; Bendazzoli, G.; Evangelisti, S.; Paulus, B. *Chem. Phys. Lett.* **2008**, *465*, 102.
(36) Vetere, V.; Monari, A.; Scemama, A.; Bendazzoli, G.; Evangelisti, S. *J. Chem. Phys.* Submitted.
(37) Pastore, M.; Monari, A.; Vetere, V.; Bendazzoli, G.; Evangelisti, S. *J. Chem. Phys.* Submitted.
(38) Vetere, V.; Monari, A.; Bendazzoli, G. L.; Evangelisti, S.; Paulus, B. *J. Chem. Phys.* **2008**, *128*, 024701.
(39) Bendazzoli, G. L.; Evangelisti, S.; Monari, A.; Paulus, B.; Vetere, V. *J. Phys. Conf. Ser.* **2008**, *117*, 012005.
(40) Knowles, P. J.; Werner, H.-J. *Chem. Phys. Lett.* **1988**, *145*, 514.
(41) Werner, H.-J.; Knowles, P. J. *J. Chem. Phys.* **1988**, *89*, 5803.
(42) Amos, R. D.; Bernhardsson, A.; Berning, A.; Celani, P.; Cooper, D. L.; Deegan, M. J. O.; Dobbyn, A. J.; Eckert, F.; Hampel, C.; Hertzer, G.; Knowels, P. J.; Korona, T.; Lindh, R.; Lloyd, A. W.; McNicholas, S. J.; Manby, F. R.; Meyer, W.; Mura, M. E.; Nicklass, A.; Palmieri, P.; Pitzer, R.; Raunhut, G.; Schütz, M.; Schumann, U.; Stoll, H.; Stone, A. J.; Tarroni, R.; Thorsteinsson, T.; Werner. H.-J. *MOLPRO*, version 2002.6; 2002.
(43) Laaksonen, L.; Anderson, S.; Boyd, K.; Häkkinen, E.; Varis, M. *gOpenMol*; Center for Scientific Computing: Espoo, Finland, 2003.
(44) Widmark, P.-O.; Malmqvist, P.-Å.; Roos, B. *Theor. Chim. Acta* **1990**, *77*, 291.
(45) Helal, W.; Evangelisti, S.; Leininger, T.; Maynau, D. *J. Comput. Chem.* **2008**, DOI: 10.1002/jcc.20982.
(46) Maynau, D.; Evangelisti, S.; Guihéry, N.; Malrieu, J. P.; Calzado, C. *J. Chem. Phys.* **2002**, *116*, 10060.
(47) Werner, H.-J.; Pflügger, K. In *Annual Reports in Computational Chemistry*; Elsevier: New York, 2006; Vol. 2, p 53.
(48) Lambert, C.; Nöll, G. *J. Am. Chem. Soc.* **1999**, *121*, 8434.

JP900663P